

Advantageous grain boundaries of iron pnictide superconductors

Takayoshi Katase¹, Yoshihiro Ishimaru², Akira Tsukamoto², Hidenori Hiramatsu¹, Toshio Kamiya¹, Keiichi Tanabe² and Hideo Hosono^{1,3,*}

¹ Materials and Structures Laboratory, Mailbox R3-1, Tokyo Institute of Technology, 4259 Nagatsuta-cho, Midori-ku, Yokohama 226-8503, Japan

² Superconductivity Research Laboratory, International Superconductivity Technology Center, 10-13 Shinonome 1-chome, Koto-ku, Tokyo 135-0062, Japan

³ Frontier Research Center, S2-6F East, Mailbox S2-13, Tokyo Institute of Technology, 4259 Nagatsuta-cho, Midori-ku, Yokohama 226-8503, Japan

(*) E-mail: hosono@mssl.titech.ac.jp

Phone: +81-45-924-5359

Fax: +81-45-924-5339

Abstract

High critical temperature superconductors have zero power consumption and could be used to produce ideal electric power lines. The principal obstacle in fabricating superconducting wires and tapes is grain boundaries—the misalignment of crystalline orientations at grain boundaries, which is unavoidable for polycrystals, largely deteriorates critical current density. Here, we report that High critical temperature iron pnictide superconductors have advantages over cuprates with respect to these grain boundary issues. The transport properties through well-defined bicrystal grain boundary junctions with various misorientation angles (θ_{GB}) were systematically investigated for cobalt-doped BaFe_2As_2 ($\text{BaFe}_2\text{As}_2:\text{Co}$) epitaxial films fabricated on bicrystal substrates. The critical current density through bicrystal grain boundary (J_c^{BGB}) remained high ($> 1 \text{ MA/cm}^2$) and nearly constant up to a critical angle θ_c of $\sim 9^\circ$, which is substantially larger than the θ_c of $\sim 5^\circ$ for $\text{YBa}_2\text{Cu}_3\text{O}_{7-\delta}$. Even at $\theta_{\text{GB}} > \theta_c$, the decay of J_c^{BGB} was much smaller than that of $\text{YBa}_2\text{Cu}_3\text{O}_{7-\delta}$.

Grain boundary (GB) engineering of high critical temperature (T_c) cuprate superconductors has been a critical issue in developing practical applications such as superconducting wires and tapes¹, because their superconducting properties heavily depend on the misorientation angle (θ_{GB}) at GBs; therefore, grains in cuprate superconductors must be highly textured to minimize deterioration of the critical current density (J_c) across misoriented GBs. In a representative cuprate superconductor, $\text{YBa}_2\text{Cu}_3\text{O}_{7-\delta}$ (YBCO), a fundamental study of intergrain J_c in bicrystal GBs (J_c^{BGB}) has been performed using several types of bicrystal substrates². Significantly misaligned adjacent grains cause J_c^{BGB} to decay exponentially as a function of θ_{GB} from 3° to 40° ³. Therefore, to produce YBCO superconducting tapes with a high J_c , it is necessary to insert well-aligned buffer layers with a small distribution of in-plane misalignment $\Delta\phi < 5^\circ$ on polycrystalline metal substrates using the ion-beam-assisted deposition (IBAD) technique⁴ or rolling-assisted biaxially textured substrates (RABiTS)⁵. Although recent progress in buffer-layer technology has established $\Delta\phi < 5^\circ$, which provides a self-field J_c of several MA/cm² at 77 K⁶, fabricating such a buffer layer is time-consuming and expensive. The development of new high- T_c and high upper critical magnetic field (B_{c2}) superconducting materials with a more gradual $J_c^{\text{BGB}}(\theta_{GB})$ dependence allows for a simple and low-cost fabrication process and provides wider flexibility in superconductor power lines and their applications.

Iron pnictide superconductors^{7,8} have received increasing interest as a new family of high- T_c superconductors because they have attractive properties such as a high T_c up to 56 K⁹ and high $B_{c2}(0)$ well over 100 T^{10,11}. The iron pnictide family shares several characteristics with the cuprates, such as a layered crystal structure, superconductivity induced by carrier doping and the presence of competing orders. However, there are

some noteworthy differences, such as the metallic nature of normal states of the iron pnictides instead of the antiferromagnetic Mott insulators of the cuprates, smaller anisotropy in superconducting properties, which is primarily due to the multi-pocket structures of their Fermi surfaces, and a highly symmetric order parameter based on s -wave instead of a d -wave pairing one¹². Therefore, we expect that these characteristics of iron pnictides would make them more favorable than cuprates with respect to the supercurrent conduction mechanism in misoriented GBs.

We have studied epitaxial films of the $A\text{EFe}_2\text{As}_2$ ($A\text{E} = \text{Sr}$ and Ba) system^{13–18} because they have considerably small anisotropy $\gamma = B_{c2}^{B\perp c} / B_{c2}^{B\parallel c} = 1.9\text{--}1.5$ in superconducting properties, high $B_{c2}(0) > 50$ T and weak thermal fluctuations with a Ginzburg number G_1 of 1.7×10^{-4} among iron pnictide materials^{19, 20}. In particular, cobalt-doped BaFe_2As_2 ($\text{BaFe}_2\text{As}_2\text{:Co}$) appears to have great potential for device applications^{15–17, 21–24} because it is rather easy to grow films by pulsed laser deposition (PLD) and chemically stable in an ambient atmosphere¹⁵. It was previously reported that in-field transport properties across bicrystal GBs (BGBs) with 4 different $\theta_{\text{GB}} = 3^\circ\text{--}24^\circ$ formed in $\text{BaFe}_2\text{As}_2\text{:Co}$ epitaxial films grown on [001]-tilt SrTiO_3 (STO) bicrystal substrates suggested that even low-angle BGB with $\theta_{\text{GB}} = 6^\circ$ obstructs supercurrent and the weak-linked BGBs exhibit a similar behavior to YBCO BGBs²². In this article, we report comprehensive results on transport properties of $\text{BaFe}_2\text{As}_2\text{:Co}$ BGB junctions grown directly on insulating bicrystal substrates in the full range of θ_{GB} from 3° to 45° . Among the results, it is particularly noteworthy that the critical angle θ_c of $\sim 9^\circ$ for $\text{BaFe}_2\text{As}_2\text{:Co}$ is much larger than the previously-reported value and the decay slope is much smaller than that of cuprates. The large θ_c allows a simpler and lower-cost fabrication process of superconducting tapes. This advantageous GB nature is

demonstrated by the high $J_c > 1 \text{ MA/cm}^2$ of a $\text{BaFe}_2\text{As}_2:\text{Co}$ superconducting tape fabricated on a polycrystalline flexible metal substrate²⁵.

Results

BaFe₂As₂:Co bicrystal grain boundary (BGB) junctions. $\text{BaFe}_2\text{As}_2:\text{Co}$ epitaxial films with the optimal Co concentration of 8% were fabricated on [001]-tilt bicrystal substrates of MgO with $\theta_{\text{GB}} = 3^\circ\text{--}45^\circ$ and (La, Sr)(Al, Ta)O₃ (LSAT) with $\theta_{\text{GB}} = 5^\circ\text{--}45^\circ$ by PLD with a Nd:YAG laser ($\lambda = 532 \text{ nm}$) at a substrate temperature of $850 \text{ }^\circ\text{C}$ ¹⁶. To date, different techniques that employ conductive buffer layers of STO, BaTiO₃²³ or Fe²⁶ have been proposed to enhance high-quality epitaxial growth. However, we have reported that it is possible to grow high-quality $\text{BaFe}_2\text{As}_2:\text{Co}$ epitaxial films with high self-field $J_c > 1 \text{ MA/cm}^2$ directly on insulating MgO and LSAT single-crystalline substrates without any buffer layer, which has been achieved by optimizing the growth conditions¹⁶. The directly grown $\text{BaFe}_2\text{As}_2:\text{Co}$ films exhibited an onset T_c of 20.7 K for MgO bicrystal substrates and 21.6 K for LSAT bicrystal substrates with sharp transition widths (ΔT_c) of 1.1 K ¹⁷.

Figure 1 (a) illustrates the device structure fabricated on [001]-tilt bicrystal substrates. To perform transport measurements of J_c^{BGB} , the $\text{BaFe}_2\text{As}_2:\text{Co}$ epitaxial films were patterned into 300- μm -long, 8- μm -wide micro-bridge structures. To compare the intergrain J_c (J_c^{BGB}) and intragrain J_c (J_c^{Grain}), two types of micro-bridges were fabricated: one was a ‘BGB junction’ that contained a BGB each, and the other was a ‘Grain bridge’ that did not contain a BGB. The electrical contacts were formed with In metal pads and Au wires. The current–voltage (I – V) characteristics of BGB junctions and Grain bridges were measured by the four-probe method.

High critical angle of strong-link – weak-link transition. The correlation between the transport J_c^{BGB} and the θ_{GB} is the most important index in characterizing the GB properties of superconductors. Figure 1 (b) summarizes the self-field $J_c^{\text{BGB}}(\theta_{\text{GB}})$ measured at 4 K and 12 K, and Figure 1 (c) shows the $J_c^{\text{BGB}}/J_c^{\text{Grain}}$ ratio at 4 K. For comparison, the generally accepted average $J_c^{\text{BGB}}(\theta_{\text{GB}})$ properties of YBCO BGB junctions measured at 4 K and 77 K² are also plotted. The J_c^{Grain} for all of the BaFe₂As₂:Co Grain bridges are greater than 1 MA/cm² at 4 K and 1.0–0.5 MA/cm² at 12 K. For the BGB junctions with low $\theta_{\text{GB}} \leq \sim 9^\circ$, the $J_c^{\text{BGB}}/J_c^{\text{Grain}}$ ratio remained almost at unity, indicating that the low-angle BGB junctions do not behave like a weak link. However, with the increase in θ_{GB} from 9° to 45° , J_c^{BGB} decreases to approximately 5%, which indicates that the transition from the strong link to the weak link occurs at θ_c of approximately 9° . In the YBCO system, the J_c^{BGB} values at 4 K for $\theta_{\text{GB}} < 5^\circ$ were slightly less than the J_c^{Grain} values, and the J_c^{BGB} values for $\theta_{\text{GB}} > 5^\circ$ showed a clear weak-link behavior^{2,27}. Although the reported data are somewhat scattered², the typical values of $\theta_c = 3\text{--}5^\circ$ are almost half the magnitude of those obtained for the BaFe₂As₂:Co BGB junctions.

Gentle J_c^{BGB} decay in weak-link regime. It is well known that the BGB junctions of the cuprates exhibit nearly exponential decay in their $J_c^{\text{BGB}}(\theta_{\text{GB}})$ curves in the weak-link regime with an empirical equation of $J_{c0}\exp(-\theta_{\text{GB}}/\theta_0)$, where θ_0 denotes the characteristic angle. The $J_c^{\text{BGB}}(\theta_{\text{GB}})$ curves are expressed by $3.0 \times 10^7 \exp(-\theta_{\text{GB}}/4.3^\circ)$ at 4 K and $7.0 \times 10^6 \exp(-\theta_{\text{GB}}/4.2^\circ)$ at 77 K. The present BaFe₂As₂:Co BGB junctions also show an exponential decay, approximated as $2.8 \times 10^6 \exp(-\theta_{\text{GB}}/9.0^\circ)$ at 4 K (the red line

in Fig. 1(b)) and $1.5 \times 10^6 \exp(-\theta_{GB}/8.5^\circ)$ at 12 K (the blue line in Fig. 1(b)). It should be noted that the θ_0 values for the BaFe₂As₂:Co BGB junctions are twice as large as those for the YBCO BGB junctions, which indicates that the $J_c^{\text{BGB}}(\theta_{GB})$ of the BaFe₂As₂:Co BGB junctions shows a more gradual decrease than that of the YBCO BGB junctions. Consequently, the J_c^{BGB} of the BaFe₂As₂:Co BGB junction exceeds that of the YBCO BGB junctions at $\theta_{GB} \geq 20^\circ$ at 4 K.

BGB junction characteristics. Figure 2 (a) shows the I - V characteristics measured at 12 K for 8- μm -wide BGB junctions with $\theta_{GB} = 4^\circ, 16^\circ$ and 45° . The BGB junction with $\theta_{GB} = 4^\circ$ only exhibits a sharp resistivity jump at a large I_c of 50 mA due to the normal state transition. Similar I - V characteristics were observed for all of the BGB junctions with $\theta_{GB} \leq 9^\circ$. On the other hand, the I - V curves of BGB junctions with $\theta_{GB} = 16^\circ$ and 45° show nonlinear characteristics without hysteresis in the low voltage region. In general, the shapes of the I - V curves of BGB junctions depend on the fractions of the Josephson current exhibiting resistively shunted junction (RSJ) behavior (W_{RSJ}) and a supercurrent showing flux flow (FF) behavior (W_{FF}). A phenomenological model to explain their fractions in I - V curves was previously proposed as follows.²⁸ I - V curves are expressed by the combination of the RSJ and the FF behaviors, where the RSJ

current follows $I_{\text{RSJ}} = \left(\left(\frac{V}{R_N} \right)^2 + I_c^2 \right)^{1/2}$ and the FF current follows

$I_{\text{FF}} = I_s - A \exp\left(-\frac{V}{V_0}\right)$ (R_N is the normal-state resistance of the barrier, and I_s , A and V_0 are constants). The fitting results based on this model drawn by the blue lines

reproduce the experimental I - V curves well. The fractions of the RSJ current W_{RSJ} are approximately 0%, 70% and 100% for the BGB junctions with $\theta_{GB} = 4^\circ, 24^\circ$ and 45° ,

respectively. The 100% RSJ current is further confirmed by good agreement with the commonly used Ambegaokar-Halperin (AH) model²⁹ drawn by the red line for the BGB junctions with $\theta_{\text{GB}} = 45^\circ$. The RSJ behavior in the I - V curves of the BGB junctions with $\theta_{\text{GB}} = 45^\circ$ was observed in the whole temperature range below T_c . The junction resistance $R_{\text{N}A}$, where A is the cross-sectional area of the junction, provides information on the nature of the barrier in BGB junctions. The $R_{\text{N}A}$ products were estimated by fitting the above-mentioned model to the experimental I - V curves²⁸. The $R_{\text{N}A}$ of the BaFe₂As₂:Co BGB junctions are $5 \times 10^{-11} \Omega\text{cm}^2$ for $\theta_{\text{GB}} = 16^\circ$ and $5 \times 10^{-10} \Omega\text{cm}^2$ for $\theta_{\text{GB}} = 45^\circ$, which are one or two orders of magnitude smaller than those of the YBCO BGB junctions (6×10^{-9} – $8 \times 10^{-8} \Omega\text{cm}^2$ for $\theta_{\text{GB}} = 16^\circ$ – 45° , respectively). These results suggest that the BaFe₂As₂:Co BGB junctions work as superconductor–normal metal–superconductor (SNS) junctions. On the other hand, the YBCO BGB junctions generally show hysteretic I - V curves at low temperatures well below T_c , indicating relatively large junction capacitances and resistances due to the insulating nature of their junction barriers. In the case of the BaFe₂As₂:Co BGB junctions, the nonhysteretic curves, even at low temperatures, suggest the metallic nature of the junction barriers.

Figures 2 (b) and (c) show the Josephson junction properties of 3- μm -wide BGB junctions with a small $\theta_{\text{GB}} = 16^\circ$ and a large $\theta_{\text{GB}} = 45^\circ$, respectively. The left figures show the magnetic field B dependencies of I_c (I_c - B) under B applied perpendicular to the film surfaces, and the right figures show the I - V curves of the BGB junctions irradiated with microwaves at a frequency of 1.39 GHz for $\theta_{\text{GB}} = 16^\circ$ and 2.0 GHz for $\theta_{\text{GB}} = 45^\circ$ measured at 16 K. The I_c - B pattern of the BGB junction with $\theta_{\text{GB}} = 45^\circ$ is distinct from the ideal Fraunhofer pattern, probably due to the inhomogeneous current distribution along the BGB; however, the junctions exhibit an I_c modulation of almost

100%, which corresponds to the fact that the BGB junction with $\theta_{GB} = 45^\circ$ exhibits the 100% RSJ current. The BGB junction with $\theta_{GB} = 16^\circ$ exhibits an I_c modulation of only 35% due to the excess current attributable to the FF current. Furthermore, both devices clearly show Shapiro steps with periodic current steps. The measured step voltage heights of 2.9 μV for $\theta_{GB} = 16^\circ$ and 4.1 μV for $\theta_{GB} = 45^\circ$ are consistent with the Josephson relation $V_{RF} = \frac{nhf_{RF}}{2e}$, where f_{RF} is the frequency of the applied microwaves.

Atomic structures of BGBs. Here, we examined the microstructure and the local chemical composition deviation of the BGBs to check the effect of an impurity phase on the weak-link junction behaviors. Figures 3 (a)–(c) show plan-view high-resolution transmission electron microscope (HR-TEM) images of the $\text{BaFe}_2\text{As}_2:\text{Co}$ BGB junctions with $\theta_{GB} = 4^\circ$, 24° and 45° , respectively. The [100]-axes of $\text{BaFe}_2\text{As}_2:\text{Co}$ are indicated by the arrows. Symmetrically tilted junctions were formed in almost the entire region of the BGBs for all of the junctions. In the BGB junctions with $\theta_{GB} = 4^\circ$ and 24° , periodic misfit dislocations at intervals of approximately 5.0 nm for $\theta_{GB} = 4^\circ$ and 1.2 nm for $\theta_{GB} = 24^\circ$ are clearly observed along the BGBs. On the other hand, the BGB with $\theta_{GB} = 45^\circ$ has blurred lattice fringes across the entire region. Using a geometric tilted boundary model, the grain boundary dislocation spacing D is given by $D = (|b|/2)/\sin(\theta_{GB}/2)$, where $|b|$ is the norm of the corresponding Burgers vector³. With the lattice constant $a = 0.396$ nm of BaFe_2As_2 ³⁰, D is estimated to be 5.7 nm and 1.0 nm for $\theta_{GB} = 4^\circ$ and 24° , respectively. The estimated D values are very similar to the D values observed above. For $\theta_{GB} = 45^\circ$, the D value is estimated to be 0.5 nm. This

value is almost the same as the lattice parameter; therefore, we cannot observe periodic misfit dislocations in the BGB with $\theta_{\text{GB}} = 45^\circ$ in Fig. 3 (c). Energy dispersive spectroscopy (EDS) line spectra across the BGBs and parallel to the BGBs confirmed that the chemical compositions of the BGBs and the film region are homogeneous, and no secondary phase was observed in the BGB regions.

Next, we discuss the relationship between θ_c and the BGB dislocation spacing D observed by TEM. For the $\text{BaFe}_2\text{As}_2:\text{Co}$ BGB junctions, the observed critical angles θ_c are approximately 9° , which correspond to a D value of approximately 2.8 nm. This is comparable to or slightly larger than the coherence length $\xi_{\text{ab}}(T)$ of 2.6 nm at 4 K estimated from the reported $\xi_{\text{ab}}(0 \text{ K}) = 2.4 \text{ nm}$ for $\text{BaFe}_2\text{As}_2:\text{Co}$ ¹⁹. The above relationship supports the notion that strong current channels still remain between the dislocations when θ_{GB} is below θ_c , while coherent superconducting current cannot pass through the BGBs at $\theta_{\text{GB}} > \theta_c$ and behaves like a weak link.

Note that there would be other factors that affect the GB transport properties. For instance, the dislocation cores formed along BGBs can produce residual strains, which have been considered to play one of the major roles in current blocking at BGBs of cuprates^{31,32}. This possibility would help us to obtain a more informative insight into the weak-link behavior in iron pnictide superconductors; however, further microstructure and strain analyses are necessary to evaluate the strain field and discuss their effects.

In-field characteristics of BGB junctions. To investigate the weak-link behavior in a B , $J_c^{\text{BGB}}(B)$ values for the BGB junctions with $\theta_{\text{GB}} = 3^\circ\text{--}45^\circ$ were measured at B up to 9 T applied parallel to the c -axis. Figure 4 (a) shows the $J_c^{\text{BGB}}(B)$ curves measured at 4 K, and the inset figure shows a magnified view in the low B region up to 0.2 T. The J_c^{Grain}

measured for the Grain bridge on the 3° MgO bicrystal substrate is also plotted by the black squares. For the BGB junctions with $\theta_{\text{GB}} = 3^\circ$ and 4° , the $J_c^{\text{BGB}}(B)$ values are almost indistinguishable from those of the $J_c^{\text{Grain}}(B)$ curves, and a reduction in J_c^{BGB} is not observed. The other BGB junctions with larger θ_{GB} show more rapid decreases than those of the $J_c^{\text{Grain}}(B)$, even in a low magnetic field. The $J_c^{\text{BGB}}(B)$ of the BGB junctions with large $\theta_{\text{GB}} = 24^\circ$ and 45° decrease sharply to 2% and 0.8% of the $J_c^{\text{Grain}}(B)$ upon the application of 0.1 T. For the BGB junctions with $\theta_{\text{GB}} = 8^\circ$ and 11° , the $J_c^{\text{BGB}}(B)$ curves show an intermediate behavior between the strongly linked and weakly linked states, where the rapid decrease in $J_c^{\text{BGB}}(B)$ at < 1 T can be attributed to the weak pinning force of the flux trapped at the dislocation cores despite the existence of strong channels with almost the same width as the coherence length $\xi_{\text{ab}}(T)$.

Metallic nature of high-angle BGB junctions. The temperature dependence of $J_c^{\text{BGB}}(J_c^{\text{BGB}}(T))$ provides more information about the nature of the barriers formed in BGBs. In general, J_c of a SNS junction follows a quadratic temperature dependence. On the other hand, a superconductor–insulator–superconductor (SIS) junction shows a linear dependence on T . Figure 4 (b) shows the $J_c^{\text{BGB}}(T)$ from T_c down to 4 K for BGB junctions with high $\theta_{\text{GB}} = 16^\circ$ – 45° . All of the $J_c^{\text{BGB}}(T)$ curves of the $\text{BaFe}_2\text{As}_2:\text{Co}$ BGB junctions show a quadratic temperature dependence as described by

$$I_c = I_0 \left(1 - \frac{T}{T_c}\right)^2 \frac{\kappa d}{\sinh(\kappa d)},$$

which is the de Gennes' theory based on a conventional proximity effect in the dirty limit³³. This relation is indicated by the orange lines in the figure, where d is the barrier thickness and κ^{-1} is the decay length for normal metal. In particular, the BGB junctions with $\theta_{\text{GB}} = 30^\circ$ and 45° have this quadratic relationship

with temperature, which is more clearly confirmed in the $J_c - \left(1 - \frac{T}{T_c}\right)^2$ plots in the inset figure. For the BGB junctions with $\theta_{\text{GB}} = 16^\circ$ and 24° , $J_c^{\text{BGB}}(T)$ deviates downward from the quadratic dependence and assumes a linear relation at temperatures lower than 10 K and 8 K, respectively. This result can be explained by the long junction limit with $w/\lambda_j > 4$ because the critical currents become so large that the Josephson penetration depth λ_j becomes smaller than the junction width w . The dependencies of the $J_c^{\text{BGB}}(T)$ curves of the $\text{BaFe}_2\text{As}_2:\text{Co}$ BGB junctions are distinctly different from those reported for the YBCO BGB junctions because the latter closely follow the linear relation $\propto \left(1 - \frac{T}{T_c}\right)$ over a wide temperature range below T_c ³⁴.

Discussion

The doubly-larger θ_c and the much gentler slope decay than those of YBCO BGB junctions make it easier to produce high J_c $\text{BaFe}_2\text{As}_2:\text{Co}$ superconducting tapes because the formation of a buffer layer with $\Delta\phi \leq 9^\circ$ is much easier than those used for the cuprates, which require much smaller $\Delta\phi$ of $< 5^\circ$, but such buffer layers have been achieved only by a few groups using an additional MgO or CeO_2 buffer layers^{35,36}. Therefore, the large θ_c allows us to use a simpler and lower-cost production process of superconducting tapes, and the iron pnictide superconducting tapes would find practical applications under a higher magnetic field if further improvement in J_c will be achieved.

The powder-in-tube technique has been rather progressing as an alternative technology for superconducting wires also in iron pnictides³⁷; however, their J_c values still remains at $\sim 10^4$ A/cm²³⁸ due probably to existence of large angle GBs with θ_{GB}

much greater than $\theta_c = 9^\circ$. The grain boundary issue in iron pnictides will be largely relaxed by the present finding. Actually, we recently succeeded in obtaining high transport $J_c = 3.5 \text{ MA/cm}^2$ with a $\text{BaFe}_2\text{As}_2:\text{Co}$ biaxially textured thin film on a polycrystalline Hastelloy tape with an IBAD-MgO textured buffer layer²⁵.

In conclusion, we fabricated high-quality $\text{BaFe}_2\text{As}_2:\text{Co}$ films with large J_c^{Grain} on bicrystal substrates with the entire range of $\theta_{\text{GB}} = 3\text{--}45^\circ$ and comprehensively examined the grain boundary nature of the iron pnictide. The primary point clarified by the present study is that the $\text{BaFe}_2\text{As}_2:\text{Co}$ BGB junctions exhibit a large θ_c of $\sim 9^\circ$. The low-angle BGBs with $\theta_{\text{GB}} \leq 9^\circ$ consist of long-period dislocation cores and, therefore, J_c^{BGB} is similar to J_c^{Grain} ; while the high-angle BGBs show a weak-link behavior with a gradual decay of $J_c^{\text{BGB}}(\theta_{\text{GB}})$ expressed by the exponential equation of $2.8 \times 10^6 \exp(-\theta_{\text{GB}}/9.0^\circ)$. Such grain boundary natures together with the high $B_{c2}(0)$ make the iron pnictides to be more promising materials for application to high J_c superconducting tapes.

Methods

Fabrication of BaFe₂As₂:Co epitaxial films on bicrystal substrates. BaFe₂As₂:Co epitaxial films were fabricated by pulsed laser deposition (PLD) on [001]-tilt bicrystal substrates of MgO with $\theta_{\text{GB}} = 3^\circ\text{--}45^\circ$ and also of LSAT with $\theta_{\text{GB}} = 5^\circ\text{--}45^\circ$. A Nd:YAG laser (wavelength: 532 nm, INDI-40, Spectra-Physics) typically used for epitaxial growth of iron pnictide films^{13,39} with a repetition rate of 10 Hz on the PLD target of a high-purity BaFe_{1.84}Co_{0.16}As₂ polycrystalline disk was used as the excitation source¹⁶. Films with 250–350 nm in thickness were grown at a temperature of 850 °C and the thickness of each film was measured precisely with a surface profiler. The base pressure in our PLD chamber was $\leq 1 \times 10^{-6}$ Pa, and film deposition was carried out in a vacuum at approximately 10^{-5} Pa. The BaFe₂As₂:Co epitaxial films grown under these conditions showed high J_c values of 1–4 MA/cm² at 4 K, which were confirmed by I – V characteristic measurements with a 1- μ V/cm criterion¹⁷.

Transport properties through BGB. The BaFe₂As₂:Co films were patterned using photolithography and Ar-ion milling into 300 μm -long and 8 μm -wide micro-bridge structures (Fig. 1(a)) to perform four-terminal I – V measurements of the J_c^{BGB} across the BGB and of the J_c^{Grain} not across the BGB and under magnetic fields perpendicular to the film surface. The critical current (I_c) and the asymptotic junction resistance (R_{NA}) were estimated from the I – V characteristics²⁸.

Microstructure and chemical composition analysis of BGB. The microstructures around the BGBs were examined by plan-view high-resolution transmission electron microscopy (HR-TEM). The TEM samples were prepared by a focused-ion-beam (FIB) micro-sampling technique in which the area near the BGBs was mechanically cutout, and that area was only thinned by FIB technique. All of the operations were performed

in a high-vacuum chamber. The chemical composition of the bulk film and the BGBs was analyzed by energy dispersive X-ray spectroscopy (EDS) with a spatial resolution of approximately 1 nm.

References

- [1] Larbalestier, D., Gurevich, A., Feldmann, D. M., Polyanskii, A. High- T_c superconducting materials for electronic power applications. *Nature* **414**, 368–377 (2001).
- [2] Hilgenkamp, H., Mannhart, J. Grain boundaries in high- T_c superconductors. *Rev. Mod. Phys.* **74**, 485–549 (2002).
- [3] Gurevich, A., Pashitskii, E. A. Current transport through low-angle grain boundaries in high-temperature superconductors. *Phys. Rev. B* **57**, 13878–13893 (1998).
- [4] Iijima, Y., Tanabe, N., Kohno, O., Ikeno, Y. In-plane aligned $\text{YBa}_2\text{Cu}_3\text{O}_{7-x}$ thin films deposited on polycrystalline metallic substrates. *Appl. Phys. Lett.* **60**, 769–771 (1992).
- [5] Goyal, A. *et al.* Epitaxial superconductors on rolling-assisted biaxially-textured substrates (RABiTS): a route towards high critical current density wire. *Appl. Supercond.* **4**, 403–427 (1996).
- [6] Yamada, Y. *et al.* Development of long length IBAD-MgO and PLD coated conductors. *IEEE Trans Appl. Supercond.* **19**, 3236–3239 (2009).
- [7] Kamihara, Y. *et al.* Iron-based layered superconductor: LaOFeP . *J. Am. Chem. Soc.* **128**, 10012–10013 (2006).
- [8] Kamihara, Y., Watanabe, T., Hirano, M., Hosono, H. Iron-based layered superconductor $\text{La}[\text{O}_{1-x}\text{F}_x]\text{FeAs}$ ($x = 0.05\text{--}0.12$) with $T_c = 26$ K. *J. Am. Chem. Soc.* **130**, 3296–3297 (2008).
- [9] Wang, C. *et al.* Thorium-doped-induced superconductivity up to 56 K in $\text{Gd}_{1-x}\text{Th}_x\text{FeAsO}$. *EPL* **83**, 67006 (2008).
- [10] Hunte, F. *et al.* Two-band superconductivity in $\text{LaFeAsO}_{0.89}\text{F}_{0.11}$ at very high magnetic field. *Nature* **453**, 903–905 (2008).

- [11] Yuan, H. Q. *et al.* Nearly isotropic superconductivity in (Ba, K)Fe₂As₂. *Nature* **457**, 565–568 (2009).
- [12] Mazin, I. I., Singh, D. J., Johannes, M. D., Du, M. H. Unconventional superconductivity with a sign reversal in the order parameter of LaFeAsO_{1-x}F_x. *Phys. Rev. Lett.* **101**, 057003 (2008).
- [13] Hiramatsu, H., Katase, T., Kamiya, T., Hirano, M., Hosono, H. Superconductivity in epitaxial thin films of Co-doped SrFe₂As₂ with bilayered FeAs structures and their magnetic anisotropy. *Appl. Phys. Express* **1**, 101702 (2008).
- [14] Hiramatsu, H., Katase, T., Kamiya, T., Hirano, M., Hosono, H. Water-induced superconductivity in SrFe₂As₂. *Phys. Rev. B* **80**, 052501 (2009).
- [15] Katase, T. *et al.* Atomically-flat, chemically-stable, superconducting epitaxial thin film of iron-based superconductor, cobalt-doped BaFe₂As₂. *Solid State Commun.* **149**, 2121–2124 (2009).
- [16] Katase, T., Hiramatsu, H., Kamiya, T., Hosono, H. High critical current density 4 MA/cm² in Co-doped BaFe₂As₂ epitaxial films grown on (La,Sr)(Al,Ta)O₃ substrates without buffer layers. *Appl. Phys. Express.* **3**, 063101 (2010).
- [17] Katase, T. *et al.* Josephson junction in cobalt-doped BaFe₂As₂ epitaxial thin films on (La,Sr)(Al,Ta)O₃ bicrystal substrates. *Appl. Phys. Lett.* **96**, 142507 (2010).
- [18] Katase, T. *et al.* DC superconducting quantum interference devices fabricated using bicrystal grain boundary junctions in Co-doped BaFe₂As₂ epitaxial films. *Supercond. Sci. Technol.* **23**, 082001 (2010).
- [19] Putti, M. *et al.* New Fe-based superconductors: properties relevant for applications. *Supercond. Sci. Technol.* **23**, 034003 (2010).
- [20] Yamamoto, A. *et al.* Small anisotropy, weak thermal fluctuations, and high field

superconductivity in Co-doped iron pnictide $\text{Ba}(\text{Fe}_{1-x}\text{Co}_x)_2\text{As}_2$. *Appl. Phys. Lett.* **94**, 062511 (2009).

[21] Iida, K. *et al.* Strong T_c dependence for strained epitaxial $\text{Ba}(\text{Fe}_{1-x}\text{Co}_x)_2\text{As}_2$ thin films. *Appl. Phys. Lett.* **95**, 192501 (2009).

[22] Lee, S. *et al.* Weak-link behavior of grain boundaries in superconducting $\text{Ba}(\text{Fe}_{1-x}\text{Co}_x)_2\text{As}_2$ bicrystals. *Appl. Phys. Lett.* **95**, 212505 (2009).

[23] Lee, S. *et al.* Template engineering of Co-doped BaFe_2As_2 single-crystal thin films. *Nat. Mater.* **9**, 397–402 (2010).

[24] Iida, K. *et al.* Scaling behavior of the critical current in clean epitaxial $\text{Ba}(\text{Fe}_{1-x}\text{Co}_x)_2\text{As}_2$ thin films. *Phys. Rev. B.* **81**, 100507 (2010).

[25] Katase, T. *et al.* Biaxially textured cobalt-doped BaFe_2As_2 films with high critical current density over 1 MA/cm^2 on MgO-buffered metal-tape flexible substrates. *Appl. Phys. Lett.* **98**, 242510 (2011)

[26] Thersleff, T. *et al.* Coherent interfacial bonding on the FeAs tetrahedron in Fe/Ba($\text{Fe}_{1-x}\text{Co}_x$) $_2\text{As}_2$ bilayers. *Appl. Phys. Lett.* **97**, 022506 (2010).

[27] Dimos, D., Chaudhari, P., Mannhart, J. Superconducting transport properties of grain boundaries in $\text{YBa}_2\text{Cu}_3\text{O}_7$ bicrystals. *Phys. Rev. B* **41**, 4038–4049 (1990).

[28] Saitoh, K., Ishimaru, Y., Fuke, H., Enomoto, Y. A model analysis for current-voltage characteristics of superconducting weak links. *Jpn. J. Appl. Phys.* **36**, L272–L275 (1997).

[29] Ambegaokar, V., Halperin, B. I. Voltage due to thermal noise in the dc Josephson effect. *Phys. Rev. Lett.* **22**, 1364–1366 (1969).

[30] Sefat, A. S. *et al.* Superconductivity at 22 K in Co-doped BaFe_2As_2 crystals. *Phys. Rev. Lett.* **101**, 117004 (2008).

- [31] Chisholm, M. F., Pennycook, S. J. Structural origin of reduced critical currents at $\text{YBa}_2\text{Cu}_3\text{O}_{7-\delta}$ grain boundaries. *Nature* **351**, 47–49 (1991).
- [32] Deutscher, G. Origin of weak-link behavior of grain boundaries in superconducting cuprates and pnictides. *Appl. Phys. Lett.* **96**, 122502 (2010).
- [33] De Gennes, P. G. Boundary effects in superconductors. *Rev. Mod. Phys.* **36**, 225–237 (1964).
- [34] Delin, K. A., Kleinsasser, A. W. Stationary properties of high-critical-temperature proximity effect Josephson junctions. *Supercond. Sci. Technol.* **9**, 227–269 (1996).
- [35] Matias, V., Hänisch, J., Rowley, E. J., Güth, K. Very fast biaxial texture evolution using high rate ion-beam-assisted deposition of MgO. *J. Mater. Res.* **24**, 125–129 (2009).
- [36] Yamada, Y. *et al.* Long IBAD-MgO and PLD coated conductor. *Physica C* **469**, 1298–1302 (2009).
- [37] Gao, Z. *et al.* Preparation of $\text{LaFeAsO}_{0.9}\text{F}_{0.1}$ wires by the powder-in-tube method. *Supercond. Sci. Technol.* **21**, 105024 (2008).
- [38] Togano, K., Matsumoto, A., Kumakura, H. Large transport critical current densities of Ag sheathed $(\text{Ba,K})\text{Fe}_2\text{As}_2+\text{Ag}$ superconducting wires fabricated by an *ex-situ* powder-in-tube process. *Appl. Phys. Express* **4**, 043101 (2011).
- [39] Hiramatsu, H., Katase, T., Kamiya, T., Hirano, M., Hosono, H. Heteroepitaxial growth and optoelectronic properties of layered iron oxyarsenide, LaFeAsO . *Appl. Phys. Lett.* **93**, 162504 (2008).

Acknowledgment

This work was supported by the Japan Society for the Promotion of Science (JSPS), Japan, through the “Funding Program for World-Leading Innovative R&D on Science and Technology (FIRST) Program”.

Author contribution

All authors equally contributed to the work presented in this paper.

Additional information

Competing financial interests: The authors declare no competing financial interests.

Figure legends

Figure 1 | Critical current density (J_c) versus misorientation angle (θ_{GB}). (a) Device structure of the BGB junctions and Grain bridges. The upper rectangular solid is an enlargement at the BGB junction. (b) Transport intergrain critical current density J_c^{BGB} in a self-field measured in BaFe₂As₂:Co BGB junctions grown on [001]-tilt bicrystal substrates of MgO (indicated by open symbols) and LSAT (closed symbols) with $\theta_{GB} = 3^\circ$ – 45° . The J_c^{BGB} of the BaFe₂As₂:Co BGB junctions were taken at 4 K (red symbols) and 12 K (blue symbols), and the red and blue solid lines are fitted to the empirical equation of $J_c^{BGB} = J_{c0}\exp(-\theta_{GB}/\theta_0)$. The average data of the YBCO BGB junctions taken at 4 K and 77 K are also indicated by the green and orange dashed lines, respectively², for comparison. (c) The ratio of the intragrain J_c (J_c^{Grain}) and J_c^{BGB} to $\theta_{GB} = 0^\circ$ – 25° at 4 K. Open and closed symbols show the ratios of samples on MgO and LSAT bicrystals, respectively. The dashed green line shows the result of the YBCO BGB junctions².

Figure 2 | Josephson junction properties. (a) Intergrain current–voltage (I – V) characteristics for the BaFe₂As₂:Co BGB junctions with $\theta_{GB} = 4^\circ$, 16° and 45° grown on MgO bicrystal substrates measured at 12 K. The experimental data are plotted by the black open circles. The red dotted lines indicate the fitted results by the A – H model based on the RSJ like transport²⁹. The blue lines show the fit to the I – V curves with the phenomenological model combining the RSJ behavior and the FF behavior²⁸. (b) and (c) Josephson junction properties at 16 K of (b) the BGB junctions with $\theta_{GB} = 16^\circ$ and (c) the BGB junctions with $\theta_{GB} = 45^\circ$. The left figures show the magnetic field (B) dependence of critical current (I_c). The B was changed along the direction of the

horizontal arrows. The right figures show the Shapiro steps under microwave irradiations at a frequency of 1.39 GHz for $\theta_{\text{GB}} = 16^\circ$ and 2.0 GHz for $\theta_{\text{GB}} = 45^\circ$.

Figure 3 | [001] plan-view HR-TEM images of the BaFe₂As₂:Co BGB junctions on MgO bicrystal substrates. The misorientation angle $\theta_{\text{GB}} =$ (a) 4° , (b) 24° , and (c) 45° . The directions of BGB junctions are indicated by dashed arrows and the [100]-axes are symmetrically tilted from the BGB lines. The misfit dislocations are marked by the down-pointing arrows. Each horizontal bar indicates 5 nm scale.

Figure 4 | Magnetic field and temperature dependence of J_c^{BGB} for the BaFe₂As₂:Co BGB junctions. (a) $J_c^{\text{BGB}}(B)$ curves of BaFe₂As₂:Co BGB junctions with $\theta_{\text{GB}} = 3^\circ$ – 45° grown on MgO bicrystal substrates measured at 4 K. The intragrain J_c (J_c^{Grain}) values measured in the Grain bridge on a 3° MgO bicrystal substrate are also plotted by closed symbols. The inset shows a magnified plot in the low magnetic field up to 0.2 T. (b) $J_c^{\text{BGB}}(T)$ for the BGB junctions with high $\theta_{\text{GB}} = 16^\circ$ – 45° grown on MgO bicrystal substrates measured from T_c down to 4 K. The orange lines show the variation of J_c with temperature as predicted from de Gennes' theory³³. The inset shows a linearized plot of the quadratic temperature dependence for $\theta_{\text{GB}} = 30^\circ$ and 45° .

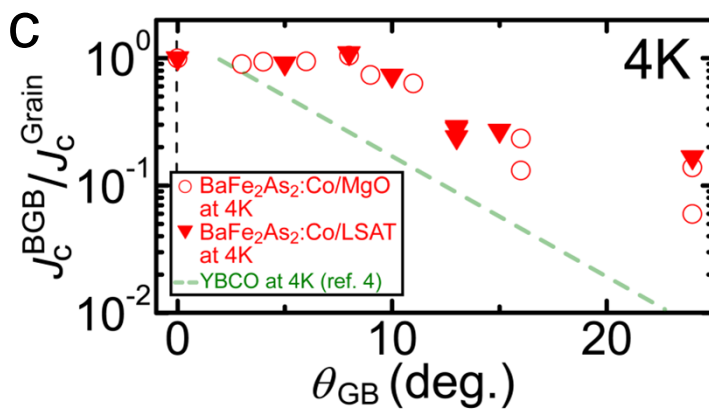
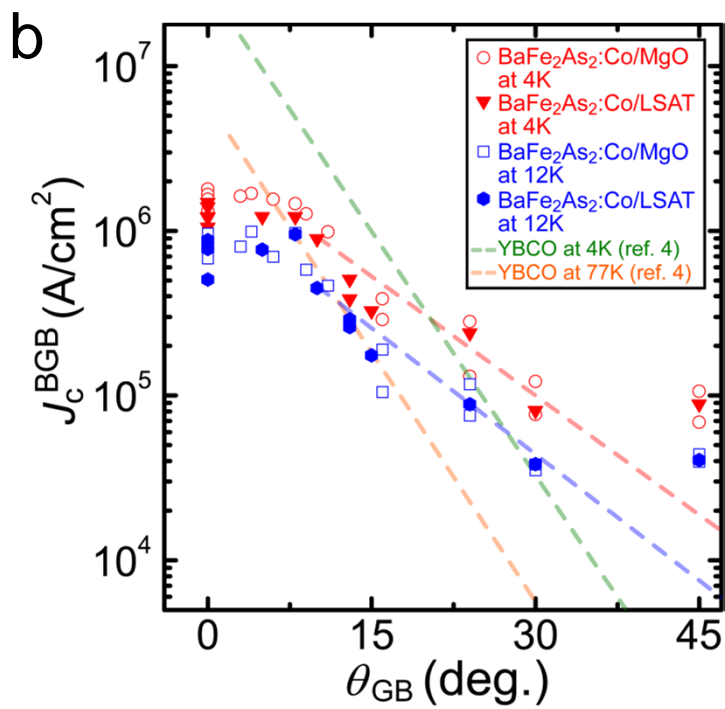
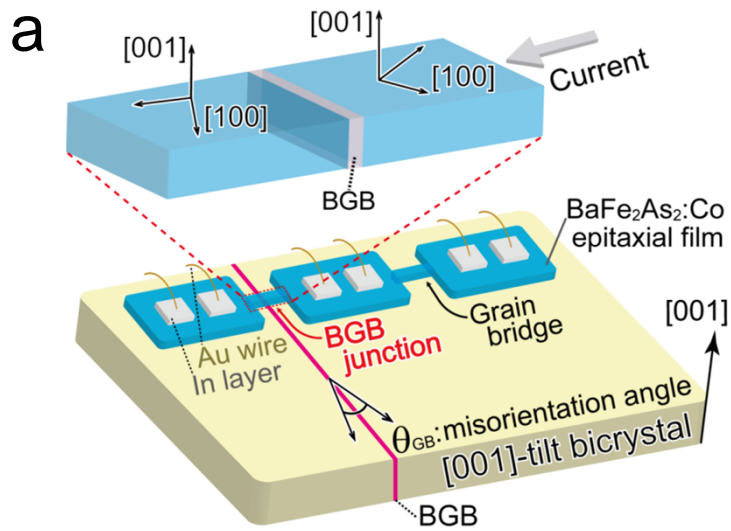
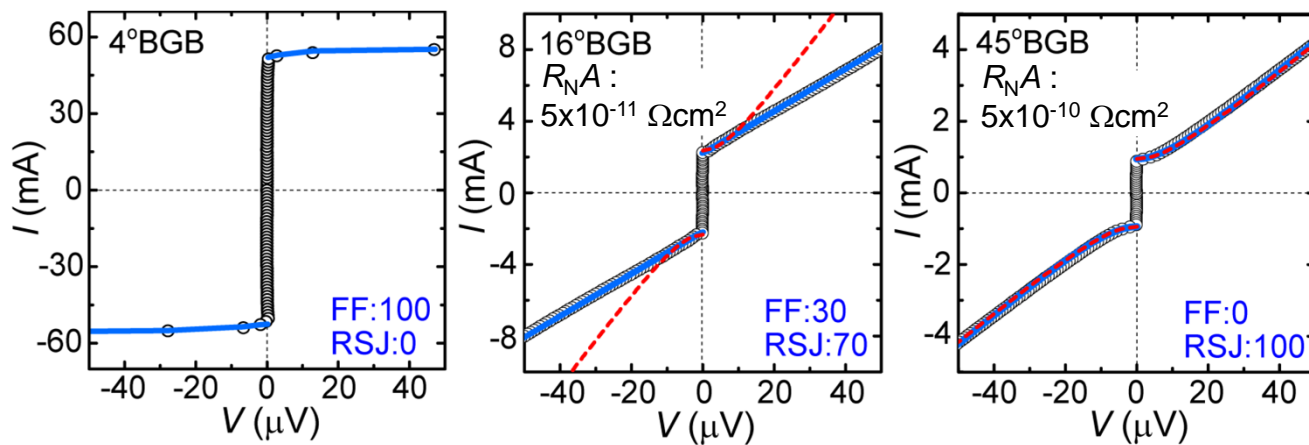
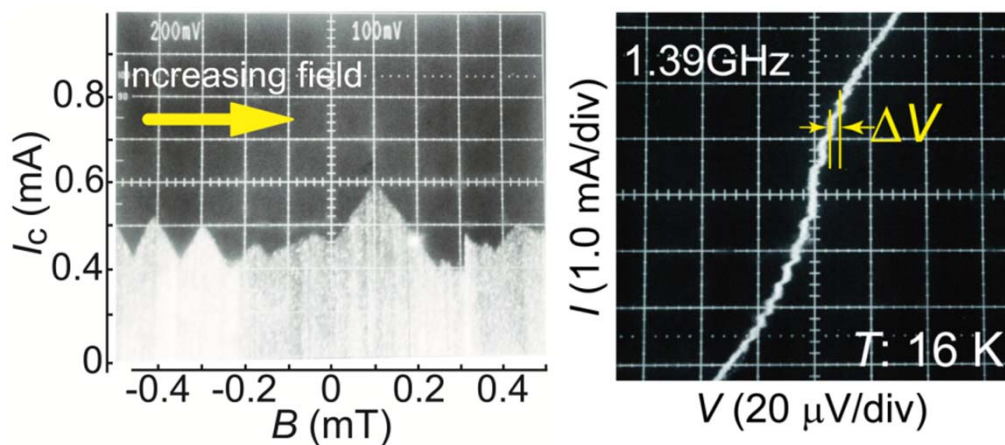
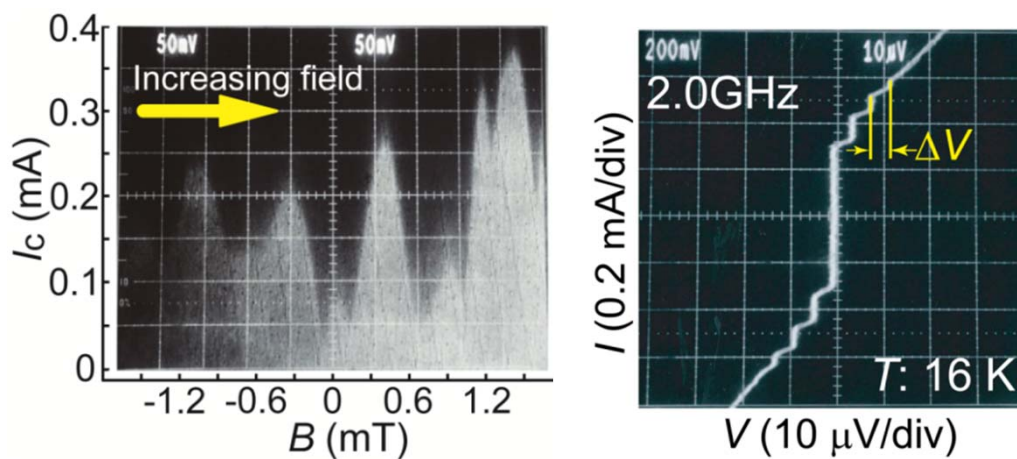


Figure 1

a**b****c****Figure 2**

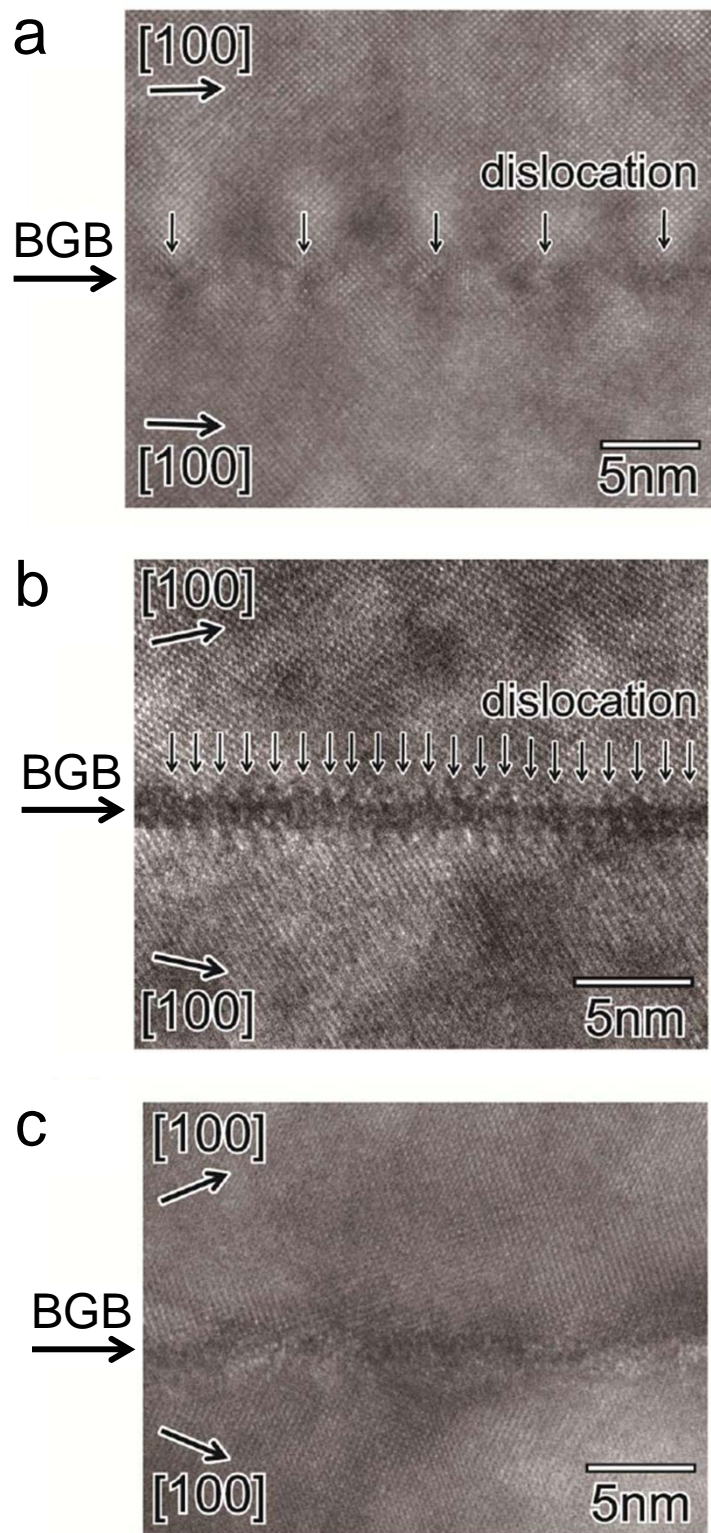


Figure 3

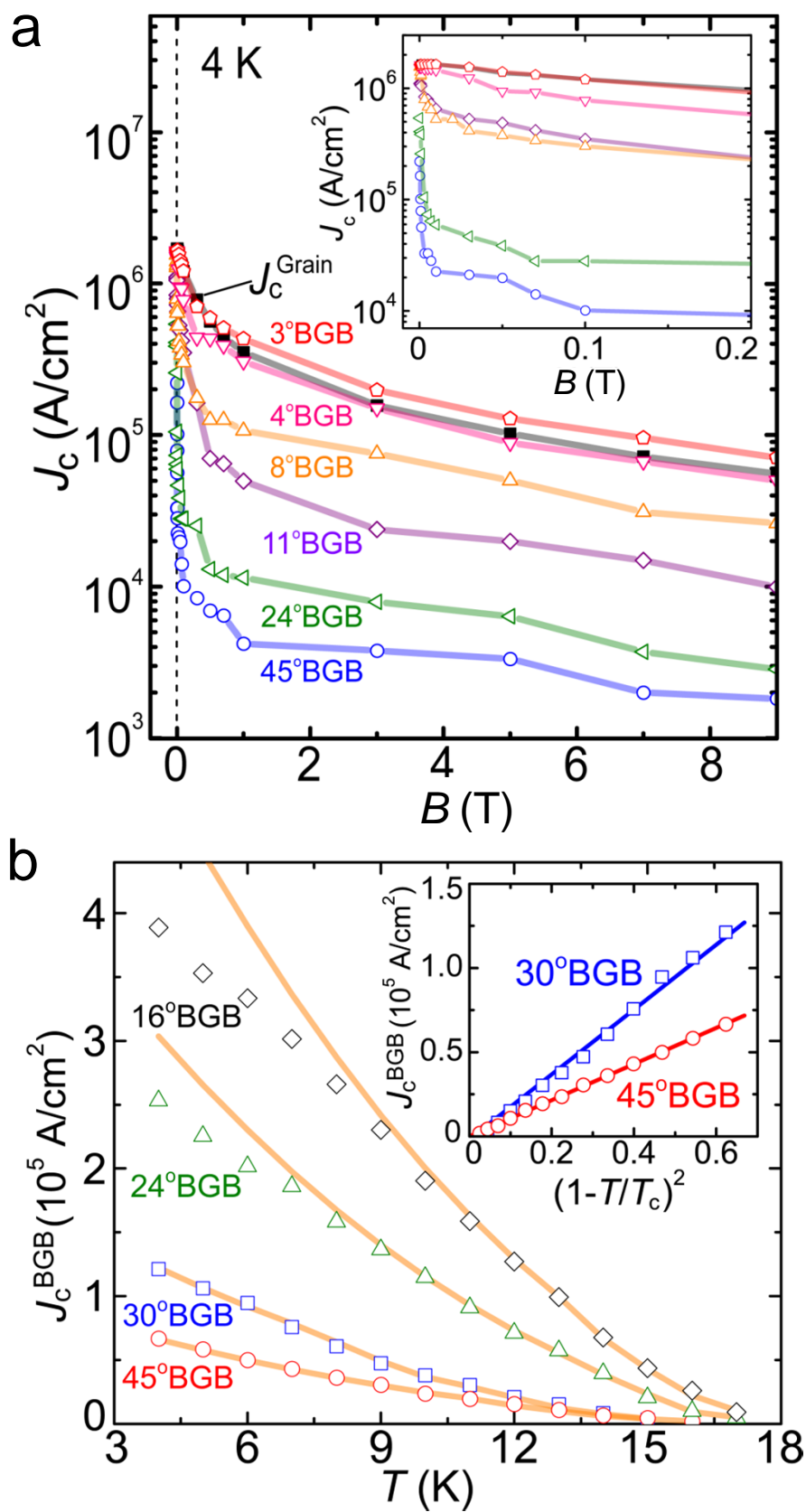


Figure 4